(Received 17 August 2024, Accepted 11 October 2024, Scheduled 21 October 2024)

Comparative Analysis of Direct Torque Control with Space Vector Modulation (DTC-SVM) and Finite Control Set-Model Predictive Control (FCS-MPC) of Five-Phase Induction Motors

Abdelfattah Hoggui[1, 2, *], Ali Benachour[2, 3], Mohamed Chafaa Madaoui[2], and Mohand Oulhadj Mahmoudi[2]

[1] *Electrotechnical Research Laboratory (ERL), Ecole Nationale Polytechnique, El Harrach, Algiers, Algeria*
[2] *Process Control Laboratory (PCL), Ecole Nationale Polytechnique, El Harrach, Algiers, Algeria*
[3] *Department of Electrical Engineering, Ecole Nationale Supérieure des Technologies Avancées, Algiers, Algeria*

ABSTRACT: This study presents a comparative analysis of Direct Torque Control with Space Vector Modulation (DTC-SVM) and Finite Control Set Model Predictive Control (FCS-MPC) applied to five-phase induction motors. Five-phase induction motors offer enhanced performance, reliability, and efficiency over traditional three-phase motors, making them suitable for high-reliability applications. The performance of DTC-SVM and FCS-MPC is evaluated through experimental implementation on a 3.5 kW five-phase induction motor, focusing on both dynamic response during speed reference changes and load variations, and static response, under steady-state conditions, as well as energy quality, specifically stator voltage and current. Experimental results show that FCS-MPC provides superior dynamic response, effectively managing speed changes and load variations, while DTC-SVM, owing to its fixed switching frequency, excels at reducing torque ripple and minimizing stator current harmonics. The choice between DTC-SVM and FCS-MPC depends on the application's needs, weighing dynamic performance, torque stability, and harmonic content. This study provides valuable insights for optimizing five-phase induction motor control and encourages future research to refine these methods or develop hybrid approaches that combine their strengths.

1. INTRODUCTION

Five-phase induction motors, unlike their traditional three-phase counterparts, feature five stator windings, providing enhanced capabilities in terms of performance and efficiency [1–3]. These motors boast several advantages, including lower current per phase, less torque ripple, better noise characteristics, potentially more torque, higher efficiency, and most importantly, superior fault tolerance compared to three-phase machines [4–7]. They are commonly employed in applications requiring high reliability and dynamic performance, such as aerospace systems, electric vehicles, marine electric propulsion, locomotive traction, and renewable energy generation [8–10].

These advantages have spurred research into adapting conventional three-phase induction motor control techniques to five-phase induction motor systems, such as Direct Torque Control-Space Vector Modulation (DTC-SVM) and Finite Control Set Model Predictive Control (FCS-MPC). Applying DTC-SVM and FCS-MPC to a five-phase induction motor introduces extra control flexibility due to the increased number of voltage vectors available from a two-level five-phase inverter, which provides 32 voltage vectors compared to just 8 in a three-phase system. This increased number of voltage vectors allows for more precise and flexible torque and flux control, minimizing the ripple amplitude of both the stator flux and the torque. Given the additional advantages of these techniques when they are applied to multiphase machines, the application of DTC-SVM and FCS-MPC to five-phase induction motors has received widespread attention in recent years.

Recent advancements in DTC-SVM have unlocked new levels of control performance and efficiency for five-phase induction motors. The research by Lu and Corzine tackles harmonic currents and torque ripple by incorporating harmonic elimination and optimal switching sequences, leading to significant improvements in both dynamic and steady-state performance [11]. Khaldi et al. investigated sensorless control approaches, comparing adaptive flux observer and model reference adaptive system (MRAS) for rotor speed estimation and highlighted the practical advantages of MRAS [12, 13]. Studies by Listwan and Pieńkowski showcase improved accuracy and smoother electromagnetic waveforms compared to traditional methods [14]. Barik and Jaladi explored integrating Artificial Neural Networks (ANNs) into the DTC-SVM framework, significantly reducing torque and flux ripple while improving speed response [15]. Furthermore, Benyoussef and Barkat explored the effectiveness of extended Kalman filters for accurate speed and flux estimation in DTC-SVM [16].

Similarly, FCS-MPC advancements are empowering five-phase induction motors with enhanced control accuracy, fault tolerance, and computational efficiency. Lim et al. explored

* Corresponding author: Abdelfattah Hoggui (abdelfettah.hoggui@g.enp.edu.dz).

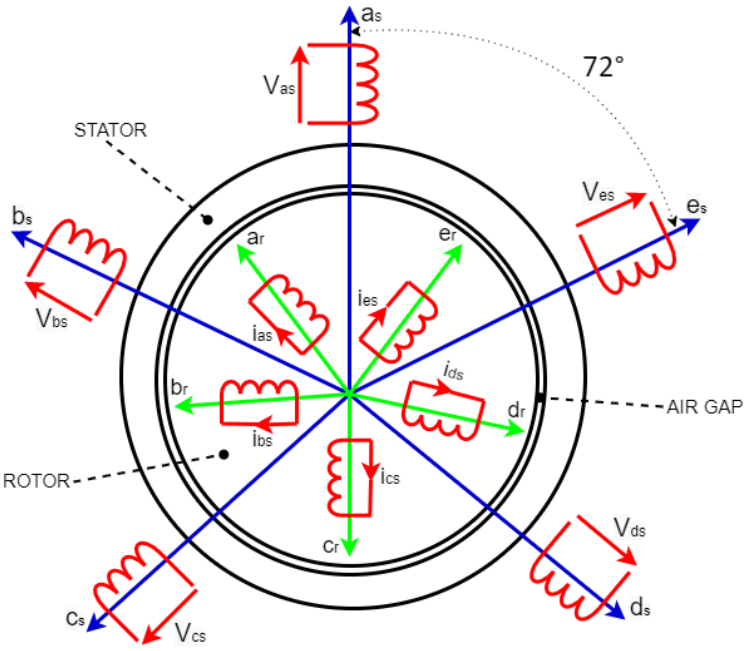

FIGURE 1. Diagram of a five-phase induction motor.

using all available switching states for optimal current control and achieving better decoupling between torque and flux currents [17]. Their research was further expanded by Lim et al., who compared FCS-MPC with traditional PI-PWM control, revealing trade-offs between transient performance and steady-state operation [18]. FCS-MPC's fault tolerance capabilities were investigated by Guzman et al., who developed a strategy to ensure seamless operation under open-phase fault conditions [19]. Martín et al. incorporated a rotor current observer into FCS-MPC, demonstrating improved prediction accuracy, reduced harmonic content, and improved current tracking performance, ultimately leading to lower torque ripple and increased overall efficiency [20]. Additionally, Guzman et al. explored reduced-order FCS-MPC approaches to minimize common-mode voltage while maintaining drive operation under varying load conditions [21].

While both DTC-SVM and FCS-MPC offer distinct advantages, there is a lack of comprehensive research directly comparing them for five-phase induction motor control. This study aims to bridge this gap by providing a comparative analysis of these two control methods. By investigating their efficiency, dynamic response, and overall performance through experimental evaluation, the research seeks to identify the strengths and weaknesses of each approach. Ultimately, this study aims to provide valuable insights into the optimal control technique for maximizing the performance of five-phase induction motors in different applications.

The organization of this paper is structured to offer a comprehensive analysis of the comparative study between DTC-SVM and FCS-MPC in five-phase induction motors. The paper begins with the modeling of the five-phase induction motor, followed by a discussion on the configuration and operation of the two-level five-phase inverter. Next, the theoretical foundations and key principles of both DTC-SVM and FCS-MPC are explored. The subsequent sections provide the experimental results, comparing the performance of DTC-SVM and FCS-MPC. Finally, the paper concludes with a summary of the findings and potential directions for future research.

2. MODELING THE FIVE-PHASE INDUCTION MOTOR

The five-phase induction motor is characterized by its five stator windings, each spatially offset by 72 degrees. This configuration is illustrated in Figure 1.

This paper relies on well-known simplifying assumptions, as described in [22, 23], to present the mathematical model of a five-phase induction motor. These assumptions include treating the magnetomotive forces as sinusoidal and assuming that the magnetic circuit is linear. The motor parameters are considered constant, and the air gap is uniform. Additionally, iron losses, such as hysteresis and eddy currents, as well as the skin effect, are neglected.

The mathematical model of the five-phase induction motor, described by differential equations in the natural phase coordinate system (a-b-c-d-e), has coefficients that change with time, as represented by systems (1) and (2) as follows [12]:

$$\begin{aligned} [V^s_{abcde}] &= [r_s]\,[I^s_{abcde}] + \frac{d\,[\Phi^s_{abcde}]}{dt} \\ [\Phi^s_{abcde}] &= [l_s]\,[I^s_{abcde}] + [l_{sr}]\,[I^r_{abcde}] \end{aligned} \tag{1}$$

$$\begin{aligned} [V^r_{abcde}] &= [r_r]\,[I^r_{abcde}] + \frac{d\,[\Phi^r_{abcde}]}{dt} \\ [\Phi^r_{abcde}] &= [l_r]\,[I^r_{abcde}] + [l_{rs}]\,[I^s_{abcde}] \end{aligned} \tag{2}$$

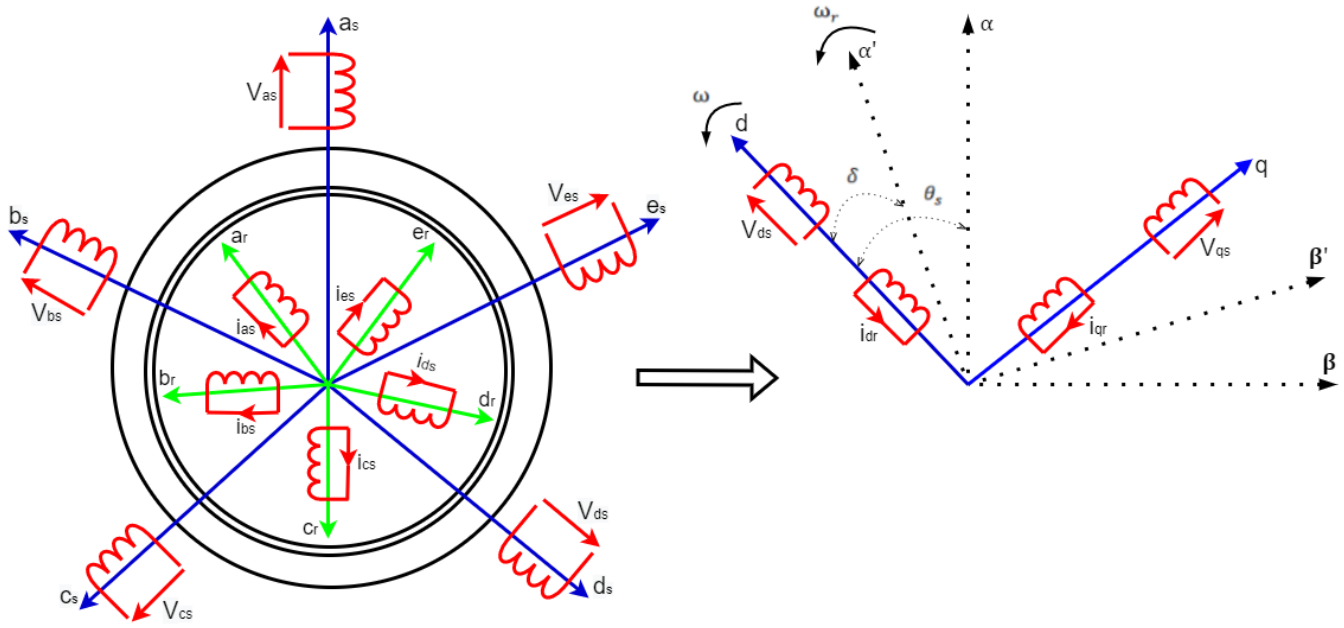

FIGURE 2. Park transformation in a five-phase induction motor.

where:

$$[V^s_{abcde}] = [V^s_a, V^s_b, V^s_c, V^s_d, V^s_e]^T$$
$$[I^s_{abcde}] = [I^s_a, I^s_b, I^s_c, I^s_d, I^s_e]^T \quad (3)$$
$$[\Phi^s_{abcde}] = [\Phi^s_a, \Phi^s_b, \Phi^s_c, \Phi^s_d, \Phi^s_e]^T$$

$$[V^r_{abcde}] = [V^r_a, V^r_b, V^r_c, V^r_d, V^r_e]^T$$
$$[I^r_{abcde}] = [I^r_a, I^r_b, I^r_c, I^r_d, I^r_e]^T \quad (4)$$
$$[\Phi^r_{abcde}] = [\Phi^r_a, \Phi^r_b, \Phi^r_c, \Phi^r_d, \Phi^r_e]^T$$

The electromagnetic torque of the motor in the (a-b-c-d-e) coordinate frame is expressed by Equation (5) as follows:

$$T_e = P\left[[I^s_{abcde}]^T \frac{d}{d\theta}\left([l_{sr}]\,[I^r_{abcde}]\right)\right] \quad (5)$$

By applying Park transformations, the stator and rotor equations are converted into the d-q-x-y-o coordinate system, simplifying the model by making the coefficients constant and time-invariant [1]. This transformation uses the matrix $P(\theta)$, known as the generalized Park matrix, derived from the Concordia matrix $[C]$ in the stationary reference frame and the rotary reference frame matrix $[D]$. This transformation conserves the instantaneous power and aligns the stator and rotor windings into electrically and magnetically equivalent windings along two perpendicular axes (d and q), as illustrated in Figure 2.

The transformations for stator and rotor variables are defined by the matrices $[P_s]$ and $[P_r]$, respectively:

$$[V^s_{dqxyo}] = [P_s]\,[V^s_{abcde}]$$
$$[I^s_{dqxyo}] = [P_s]\,[I^s_{abcde}] \quad (6)$$
$$[\Phi^s_{dqxyo}] = [P_s]\,[\Phi^s_{abcde}]$$

$$[V^r_{dqxyo}] = [P_r]\,[V^r_{abcde}]$$
$$[I^r_{dqxyo}] = [P_r]\,[I^r_{abcde}] \quad (7)$$
$$[\Phi^r_{dqxyo}] = [P_r]\,[\Phi^r_{abcde}]$$

After applying these transformations, the equations governing the voltages and fluxes of the five-phase induction motor in a reference frame rotating at arbitrary speed ω are summarized by systems (8) and (9) as follows:

$$V_{ds} = R_s I_{ds} + \frac{d\Phi_{ds}}{dt} - \omega\Phi_{qs}$$
$$\Phi_{ds} = (L_{ls} + L_m) I_{ds} + L_m I_{dr}$$
$$V_{qs} = R_s I_{qs} + \frac{d\Phi_{qs}}{dt} + \omega\Phi_{ds}$$
$$\Phi_{qs} = (L_{ls} + L_m) I_{qs} + L_m I_{qr}$$
$$V_{xs} = R_s I_{xs} + \frac{d\Phi_{xs}}{dt}$$
$$\Phi_{xs} = L_{ls} I_{xs}$$

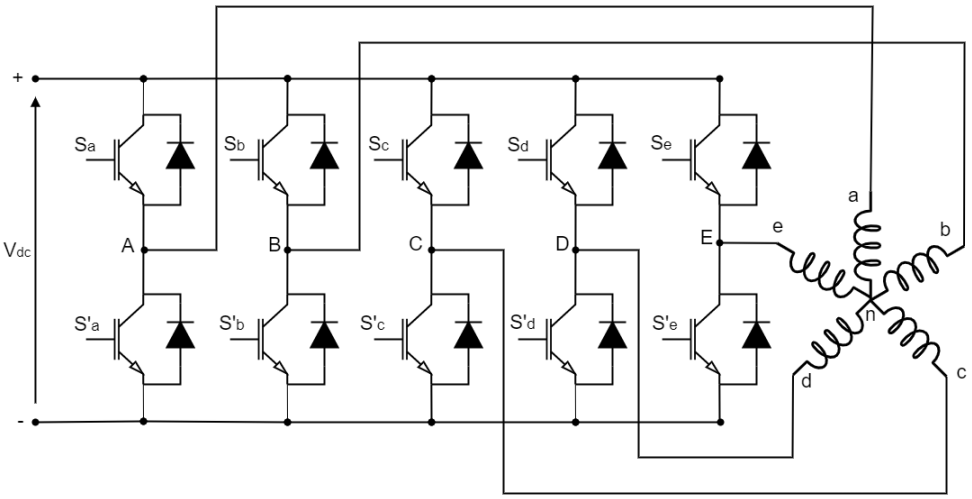

FIGURE 3. Circuit of a five-phase voltage source inverter.

$$
\begin{aligned}
V_{ys} &= R_s I_{ys} + \frac{d\Phi_{ys}}{dt} \\
\Phi_{ys} &= L_{ls} I_{ys} \\
V_{os} &= R_s I_{os} + \frac{d\Phi_{os}}{dt} \\
\Phi_{os} &= L_{ls} I_{os}
\end{aligned} \tag{8}
$$

$$
\begin{aligned}
V_{dr} &= R_r I_{dr} + \frac{d\Phi_{dr}}{dt} - (\omega - \omega_r)\Phi_{qr} \\
\Phi_{dr} &= (L_{lr} + L_m) I_{dr} + L_m I_{ds} \\
V_{qr} &= R_r I_{qr} + \frac{d\Phi_{qr}}{dt} + (\omega - \omega_r)\Phi_{dr} \\
\Phi_{qr} &= (L_{lr} + L_m) I_{qr} + L_m I_{qs} \\
V_{xr} &= R_r I_{xr} + \frac{d\Phi_{xr}}{dt} \\
\Phi_{xr} &= L_{lr} I_{xr} \\
V_{yr} &= R_r I_{yr} + \frac{d\Phi_{yr}}{dt} \\
\Phi_{yr} &= L_{lr} I_{yr} \\
V_{or} &= R_r I_{or} + \frac{d\Phi_{or}}{dt} \\
\Phi_{or} &= L_{lr} I_{or}
\end{aligned} \tag{9}
$$

The electromagnetic torque developed by the motor, after the transformation, is expressed by Equation (10) as follows:

$$
T_{em} = p\left(\Phi_{ds} i_{qs} - \Phi_{qs} i_{ds}\right) \tag{10}
$$

From Equations (8) and (9), it is apparent that the key difference between the five-phase motor model and the three-phase motor model is the existence of x-y components in the d-q-x-y-o coordinate system, which are not present in the three-phase model. The stator and rotor voltages in the x-y frame depend only on their respective currents and fluxes, without involving components from each other (i.e., the x components do not include terms from y), and without involving the d-q components. Similarly, the stator and rotor fluxes in the x-y frame are determined solely by their respective currents, without coupling between stator and rotor components. The rotor and stator components in the x-y frame are fully decoupled from the components in the d-q frame and from each other, and therefore do not contribute to the production of flux or electromagnetic torque, although they can introduce additional losses in the motor [12, 14–16, 20, 24]. However, for the purposes of this study, these losses are considered negligible, as supported by previous research [12, 23, 25].

Furthermore, given the short-circuited rotor winding and the star configuration of the stator winding, and assuming that the five-phase components are balanced within both the stator and rotor, the zero-sequence components in both the stator and rotor windings can be ignored. Consequently, the analysis can focus primarily on the d-q components, which are responsible for flux and torque production.

As a result, the model of the five-phase induction motor, under the given assumptions, effectively reduces to that of a three-phase induction motor. This reduction, as noted in several studies [12, 13, 15], simplifies the implementation of traditional three-phase control methods, such as DTC-SVM and FCS-MPC, to five-phase motors without impacting the accuracy of the results.

3. TWO-LEVEL FIVE-PHASE INVERTER

In this study, a two-level five-phase inverter is utilized to power a five-phase induction motor, as shown in Figure 3. The inverter operates with a constant DC voltage input. Each leg of the inverter includes two IGBTs, which are controlled in a com-

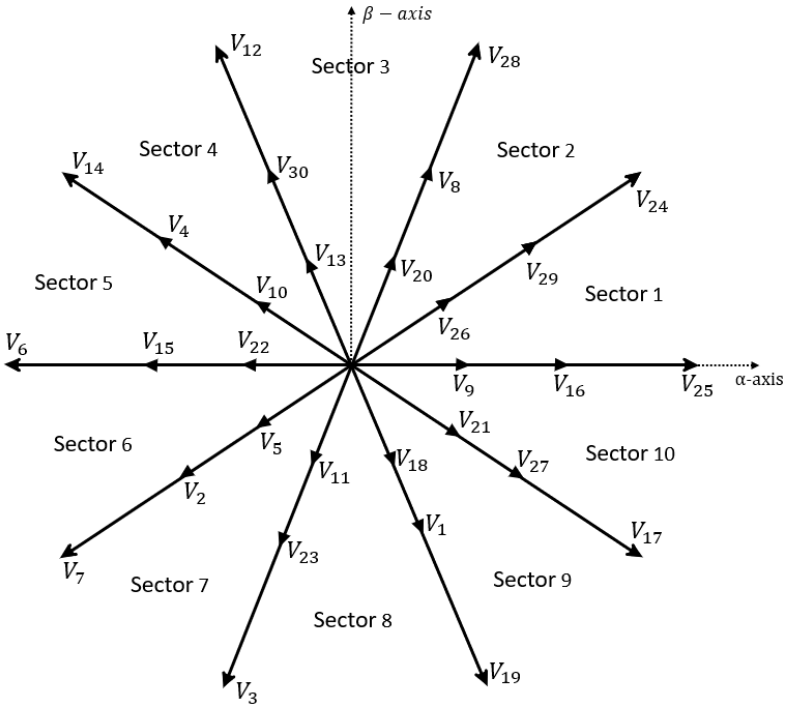

FIGURE 4. Space voltage vectors of the two-level five-phase inverter (α-β Plane).

plementary manner to avoid short circuits in the DC bus and ensure continuous current flow to the load.

The inverter's output voltage is governed by the switching states of the IGBTs. Given that each leg contains two IGBTs, there are 2^5 (32) possible switching states, resulting in 32 space voltage vectors. These vectors include two zero vectors and thirty active vectors, which have three distinct amplitudes and are distributed across ten 36-degree sectors, as illustrated in Figure 4.

4. DIRECT TORQUE CONTROL WITH SPACE VECTOR MODULATION FOR A FIVE-PHASE INDUCTION MOTOR

This work employs a DTC-SVM scheme that utilizes a closed-loop control of torque and stator flux in the stator flux reference frame. Figure 5 depicts the control structure, which relies on two PI-type controllers for both torque and stator flux control [26].

The control strategy relies on a simplified description of the stator voltage components presented in the stator flux coordinate system ($\Phi_{ds} = \Phi_s, \Phi_{qs} = 0$). Consequently, the equations of the stator voltage from system (8) and torque expressions (10) will be presented as follows:

$$\begin{aligned} V_{ds} &= R_s I_{ds} + \frac{d\Phi_s}{dt} \\ V_{qs} &= R_s I_{qs} + \omega \Phi_s \\ T_e &= p \Phi_s I_{qs} \end{aligned} \tag{11}$$

Neglecting the voltage drop across the stator resistance (R_s), system (11) reveals that the V_{ds} component primarily influences the stator flux amplitude variation, while the V_{qs} component governs torque control. The outputs from the PI controllers for flux and torque represent the reference stator voltage components (V_{ds} and V_{qs}) in the stator flux reference frame, as shown in Figure 6. These reference voltages are then transformed to the stationary α-β reference frame to enable SVM implementation for voltage synthesis.

This study employs an SVM strategy that utilizes four active space vectors (two medium and two large) within each sector to generate the desired reference voltage at each sampling time step [27, 28]. The application times for the large vectors T_{al} and T_{bl} and for the medium vectors T_{am} and T_{bm} are calculated using the following formulas [28]:

$$\begin{aligned} T_{al} &= \frac{|V_l| \sin\left(\frac{\pi k}{5} - \alpha\right)}{|V_l| + |V_m| \sin\left(\frac{\pi}{5}\right)} \cdot T_s, \\ T_{bl} &= \frac{|V_l| \sin\left(\alpha - \frac{(k-1)\pi}{5}\right)}{|V_l| + |V_m| \sin\left(\frac{\pi}{5}\right)} \cdot T_s \end{aligned} \tag{12}$$

$$\begin{aligned} T_{am} &= \frac{|V_m| \sin\left(\frac{\pi k}{5} - \alpha\right)}{|V_l| + |V_m| \sin\left(\frac{\pi}{5}\right)} \cdot T_s, \\ T_{bm} &= \frac{|V_m| \sin\left(\alpha - \frac{(k-1)\pi}{5}\right)}{|V_l| + |V_m| \sin\left(\frac{\pi}{5}\right)} \cdot T_s \end{aligned} \tag{13}$$

The application time of the zero voltage vector T_o is calculated as:

$$T_o = T_s - T_{al} - T_{am} - T_{bl} - T_{bm} \tag{14}$$

where:

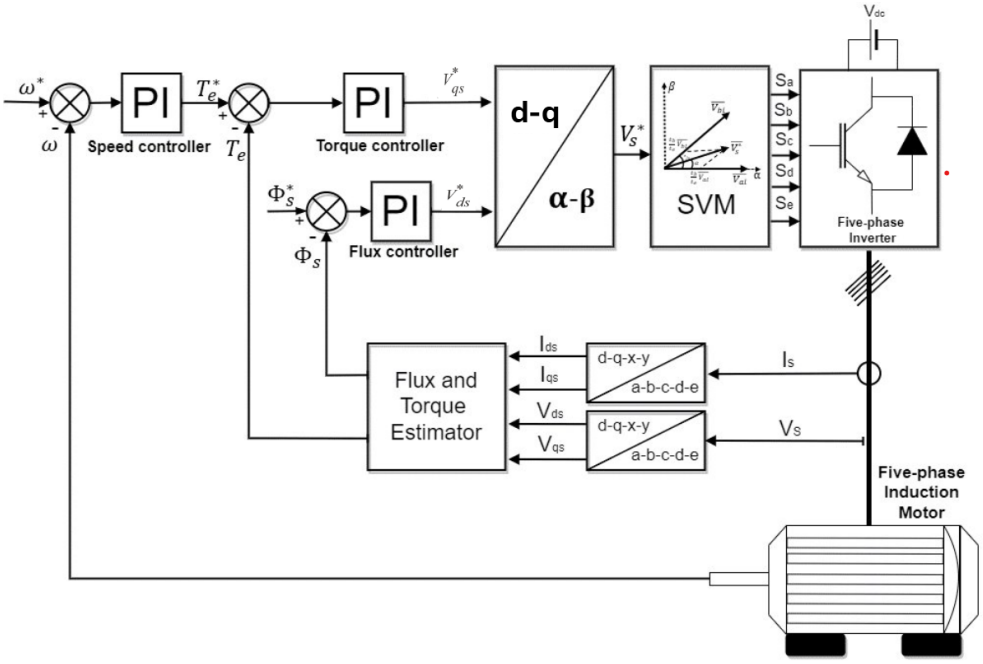

FIGURE 5. Block diagram of DTC-SVM.

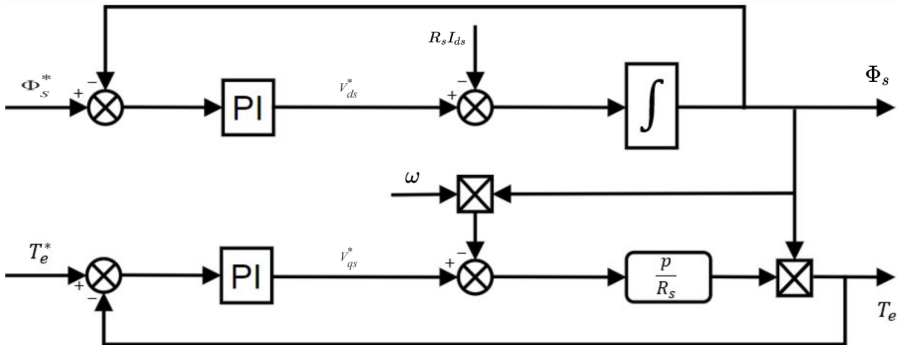

FIGURE 6. Closed loop of the regulation.

- k is the sector number ranging from 1 to 10.
- T_s represents the switching period.
- $|V_l|$ and $|V_m|$ are the magnitudes of the large and medium voltage vectors, respectively, given by:
  - $|V_l| = \sqrt{\frac{2}{5}V_{DC}^2 \cos\left(\frac{\pi}{5}\right)}$
  - $|V_m| = \sqrt{\frac{2}{5}V_{DC}}$

These calculated times determine the precise moments during the switching period when each vector is activated. Initially, the first zero vector is applied for $\frac{T_o}{4}$. Following this, the sequence involves the activation of the first medium vector V_{am} for $\frac{T_{am}}{2}$, followed by the first large vector V_{bl} for $\frac{T_{bl}}{2}$. Next, the second large vector V_{al} is applied for $\frac{T_{al}}{2}$, and then the second medium vector V_{bm} is applied for $\frac{T_{bm}}{2}$. At the midpoint of the switching period, the second zero vector is applied for $\frac{T_o}{2}$, marking the transition to the second half of the cycle. This second half mirrors the first, with V_{bm}, V_{al}, V_{bl}, and V_{am} being applied in sequence, followed by the application of the first zero vector for $\frac{T_o}{4}$ at the end of the cycle. This pattern, as illustrated in Figure 7, is consistently repeated for each sector.

5. FINITE CONTROL SET MODEL PREDICTIVE CONTROL FOR A FIVE-PHASE INDUCTION MOTOR

The block diagram of FCS-MPC for a five-phase induction motor is shown in Figure 8. This diagram illustrates the control loop, including the prediction model, cost function evaluation, and the selection of optimal switching states.

In the context of a five-phase induction motor, FCS-MPC utilizes the mathematical model of the motor in the stationary reference frame to predict future states, including stator currents and stator and rotor flux linkages, based on possible switching states of the inverter. The process involves discretizing the

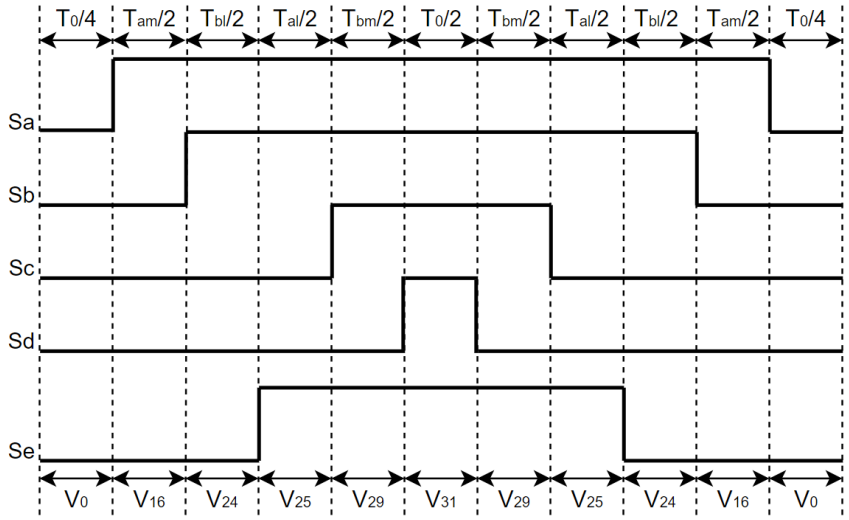

FIGURE 7. Inverter switching states for sector 1.

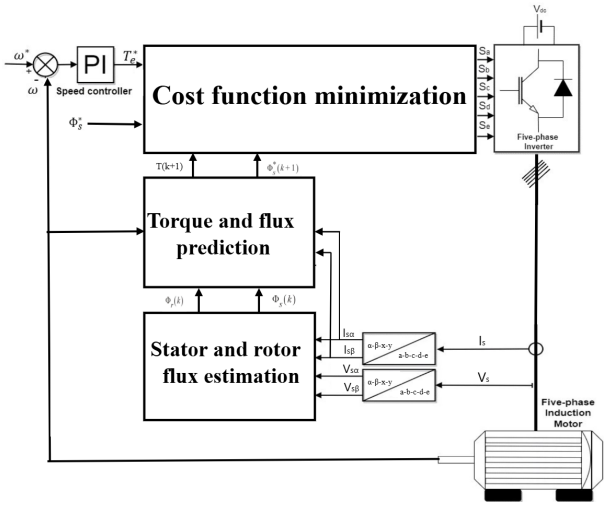

FIGURE 8. Block diagram of FCS-MPC.

motor's dynamic equations and using these discrete models to forecast the motor's behavior over a short prediction horizon. At each sampling interval, the controller evaluates the predicted states for all potential voltage vectors (switching combinations of the five-phase inverter) and computes a cost function that typically includes terms for tracking errors [29].

The continuous-time model given in system (8) in a reference frame rotating at an arbitrary speed ω can be transformed into the stationary reference frame (α-β-x-y-o) and discretized using the sampling period T_s for digital control implementation. In this study, only the α-β components are considered for simplification purposes. The resulting equations for the stator flux linkages in discrete form are:

$$\begin{aligned}\Phi_{s\alpha}[k+1] &= \Phi_{s\alpha}[k] + T_s\left(V_{s\alpha}[k] - R_s I_{s\alpha}[k]\right)\\ \Phi_{s\beta}[k+1] &= \Phi_{s\beta}[k] + T_s\left(V_{s\beta}[k] - R_s I_{s\beta}[k]\right)\end{aligned} \tag{15}$$

The equations for the rotor flux linkages in discrete form are:

$$\begin{aligned}\Phi_{r\alpha}[k+1] =&(1-\frac{R_r T_s}{L_r})\Phi_{r\alpha}[k] + T_s\omega_m\Phi_{r\beta}[k]\\ &+\frac{R_r T_s L_m}{L_r} I_{s\alpha}[k]\\ \Phi_{r\beta}[k+1] =&(1-\frac{R_r T_s}{L_r})\Phi_{r\beta}[k]\\ &- T_s\omega_m\Phi_{r\alpha}[k] + \frac{R_r T_s L_m}{L_r} I_{s\beta}[k]\end{aligned} \tag{16}$$

The expressions for the rotor currents in terms of the rotor flux linkages are:

$$\begin{aligned}I_{r\alpha}[k+1] &= \frac{\Phi_{r\alpha}[k+1] - L_m I_{s\alpha}[k+1]}{L_r}\\ I_{r\beta}[k+1] &= \frac{\Phi_{r\beta}[k+1] - L_m I_{s\beta}[k+1]}{L_r}\end{aligned} \tag{17}$$

The stator flux linkages in terms of stator and rotor currents are given by:

$$\begin{aligned}\Phi_{s\alpha}[k+1] &= L_s I_{s\alpha}[k+1] + L_m I_{r\alpha}[k+1] \\ \Phi_{s\beta}[k+1] &= L_s I_{s\beta}[k+1] + L_m I_{r\beta}[k+1]\end{aligned} \tag{18}$$

Finally, the stator currents are updated as follows:

$$\begin{aligned}I_{s\alpha}[k+1] &= \left(1+\frac{T_s}{\tau_\sigma}\right) I_{s\alpha}[k] \\ &+ \frac{T_s}{\tau_\sigma}\left(\frac{1}{R_\sigma}\left(\frac{k_r}{\tau_r}\Phi_{r\alpha}[k] + k_r\omega_m\Phi_{r\beta}[k]\right) + V_{s\alpha}[k]\right) \\ I_{s\beta}[k+1] &= \left(1+\frac{T_s}{\tau_\sigma}\right) I_{s\beta}[k] \\ &+ \frac{T_s}{\tau_\sigma}\left(\frac{1}{R_\sigma}\left(\frac{k_r}{\tau_r}\Phi_{r\beta}[k] - k_r\omega_m\Phi_{r\alpha}[k]\right) + V_{s\beta}[k]\right)\end{aligned} \tag{19}$$

where:

- $\sigma = 1 - \frac{L_m^2}{L_r L_s}$
- $\tau_\sigma = \frac{\sigma L_s}{R_\sigma}$
- $k_r = \frac{L_m}{L_r}$
- $\tau_r = \frac{L_r}{R_r}$
- $R_\sigma = R_s + k_r^2 R_r$
- ω_m is the mechanical angular speed

The future electromagnetic torque is predicted using the equations:

$$T_e[k+1] = \frac{5}{2} p \left(\Phi_{s\alpha}[k+1] I_{s\beta}[k+1] - \Phi_{s\beta}[k+1] I_{s\alpha}[k+1]\right) \tag{20}$$

The cost function used in this study focuses on minimizing the error in torque and stator flux, ensuring precise control of the motor. The cost function is given by:

$$J = \lambda_T \left|T_e[k+1] - T_{\text{ref}}\right| + \lambda_\Phi \left|\Phi_s[k+1] - \Phi_{s,\text{ref}}\right| \tag{21}$$

where:

- λ_T and λ_Φ are weighting factors for the torque and flux errors, respectively.
- $T_e[k+1]$ is the predicted electromagnetic torque at the next time step.
- T_{ref} is the reference torque.
- $\Phi_s[k+1]$ is the predicted stator flux magnitude at the next time step.
- $\Phi_{s,\text{ref}}$ is the reference stator flux magnitude.

The control action that minimizes the cost function is applied to the inverter. This involves evaluating all 32 possible voltage vectors and choosing the one that results in the lowest cost. This optimization ensures minimal tracking error and efficient control. By minimizing the cost function at each sampling step, FCS-MPC ensures optimal performance with minimal tracking error.

6. RESULTS

This section presents the experimental results obtained from testing the proposed DTC-SVM and FCS-MPC control strategies on a five-phase induction motor. The experimental setup was implemented on a test bench, as shown in Figure 9, and the detailed parameters for the motor and control settings are provided in Appendix Table A1.

The test bench comprises two main components: the power part and the control part.

The power part includes a 3.5 kW five-phase induction motor coupled with a direct current generator, which functions as a load. The generator is connected to adjustable resistors, allowing for manual modification of the total resistance to vary the load torque. The motor is powered by two three-phase inverters from Semikron, which receive a fixed 450 V DC input voltage from a diode rectifier fed by an autotransformer.

The control part utilizes a DS1104 control board from dSPACE GmbH, installed within a computer. The control algorithms for both DTC-SVM and FCS-MPC are implemented using MATLAB/Simulink and ControlDesk software. MATLAB/Simulink facilitates real-time application programming through Real-Time Interface toolbox blocks. These validated programs are then automatically compiled and downloaded to the board using dSPACE ControlDesk Manager software. ControlDesk provides a graphical interface for controlling signals and real-time visualization from the Simulink environment. An external connection box (dSPACE CLP1104 Connector Panel) ensures data exchange between the power and control parts. Additionally, there is an interface for conditioning control signals and a measurement environment equipped with various sensors. The measurement environment includes an incremental encoder for speed measurement and LEM current sensors for current measurement.

The DTC-SVM and FCS-MPC control strategies were evaluated under various conditions to compare their static and dynamic performances. Static performance was assessed by examining behavior under steady-state conditions, focusing on metrics such as torque ripple, total harmonic distortion (THD) of current, and steady-state error. Dynamic performance evaluation involved analyzing responses to changes in operating conditions, such as variations in speed or load, with key metrics including response time, overshoot, settling time, and stability. The experimental results, presented in Figures 10 to 15, provide valuable insights into the robustness and effectiveness of each control strategy in various operational scenarios.

Figure 10 presents the mechanical and electromagnetic variables observed during the experimental test, including speed, torque, and stator flux. The speed references change from -100

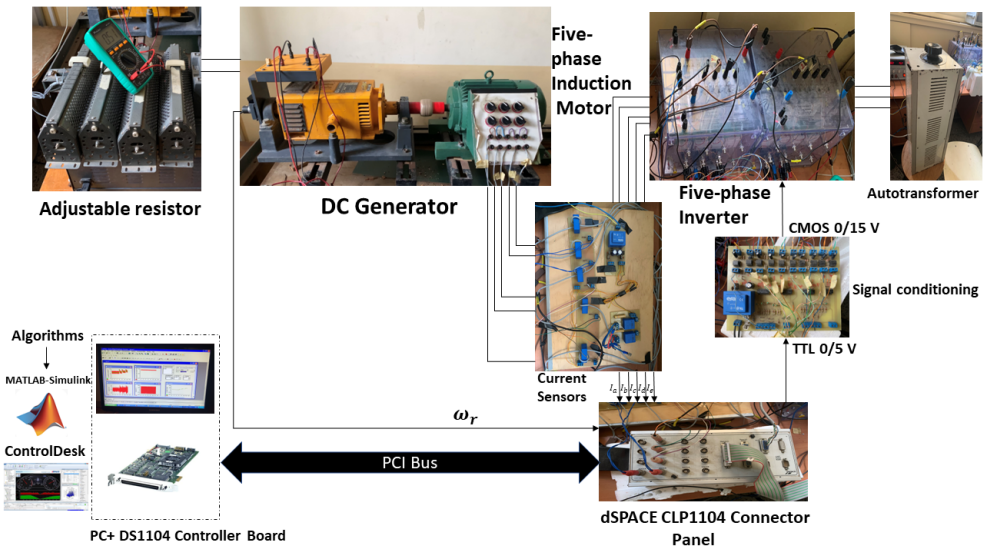

FIGURE 9. Diagram of the experimental setup.

to 150 rad/s, increasing by 50 rad/s at each step under the same load conditions.

In Figure 10(a) and Figure 10(b), the actual speed precisely follows its reference for both DTC-SVM and FCS-MPC, with observed oscillations due to the precision of the incremental encoder for speed, rather than a direct indicator of performance. The response time for DTC-SVM is 1 second for -100 to -50 rad/s and 1.55 seconds for 50 to 100 rad/s, while FCS-MPC takes 0.73 seconds and 1.14 seconds, respectively, indicating FCS-MPC's faster response. Both strategies show no overshoot, ensuring stability and control precision.

In Figure 10(c) and Figure 10(d), the actual torque precisely follows its reference for both DTC-SVM and FCS-MPC. In steady state, torque ripple varies with reference speed. The FCS-MPC strategy exhibits higher torque ripple, with the maximum average torque ripple reaching 0.5157 Nm, indicating less smooth torque control. In contrast, the DTC-SVM strategy demonstrates superior torque control, with a maximum average torque ripple of 0.2472 Nm, resulting in a smoother and more stable torque response.

In Figure 10(e) and Figure 10(f), the stator flux magnitude closely follows its reference value for both control strategies. For DTC-SVM, there are minor deviations from the reference flux, particularly when changing speed, indicating slight instability in maintaining the desired flux level. These fluctuations result in a ripple reaching up to 0.05 Wb throughout the test. In contrast, the MPC strategy maintains the flux ripple below 0.01 Wb throughout the test, even with speed variations, demonstrating superior control accuracy and stability.

Figure 11 presents the stator current observed when the speed changes from 50 to 150 rad/s. For both control strategies, the stator currents exhibit increases in both magnitude and frequency as the speed increases. During the transient state, the peak current for DTC-SVM reaches 3.3 A, while for FCS-MPC it reaches 5 A. The waveforms of the stator current in DTC-SVM are closer to a sinusoidal shape, whereas the waveforms in FCS-MPC show more variability. This difference is attributed to the fact that DTC-SVM operates with a fixed switching frequency. In contrast, FCS-MPC operates with a variable switching frequency, compounded by the limitations imposed by the fixed step size of the solver, which is set to 10^{-4} in the experimental bench.

Figures 12 and 13 illustrate the stator current, the x-y current components, and the output voltage waveforms of the five-phase inverter, along with their Fast Fourier Transform (FFT), for both DTC-SVM and FCS-MPC. The motor speed is fixed at 200 rad/s under the same load conditions. These FFT analyses highlight a distinct contrast in the harmonic content of both current and voltage waveforms.

For the stator current, the DTC-SVM demonstrates a lower Total Harmonic Distortion (THD) of 15.30%, whereas the FCS-MPC exhibits a higher THD of 22.85%. A closer examination of the harmonic content shows that, for DTC-SVM, the third harmonic has a magnitude of 0.046, which is approximately 3.52% of the fundamental, and the fifth harmonic has a magnitude of 0.045, which is approximately 3.49% of the fundamental. In contrast, the FCS-MPC exhibits higher magnitudes for the same harmonics, the third harmonic has a magnitude of 0.064, which is approximately 4.59% of the fundamental, and the fifth harmonic has a magnitude of 0.078, which is approximately 5.59% of the fundamental. The higher THD in the FCS-MPC is attributed to the variable switching frequency, which leads to increased low-frequency harmonic content in the stator current, making the x-y current components more significant and not as effectively managed as in DTC-SVM. This suggests that the DTC-SVM control, with its fixed switching frequency, is more effective in minimizing harmonic distortion for the stator current.

For the output voltage, the DTC-SVM shows a higher THD of 133.49%, whereas the FCS-MPC exhibits a lower THD of 94.33%. A closer examination reveals that, for DTC-SVM, there are numerous significant harmonics with high magnitudes, particularly among the medium-frequency and high-frequency harmonics. However, these high-frequency harmon-

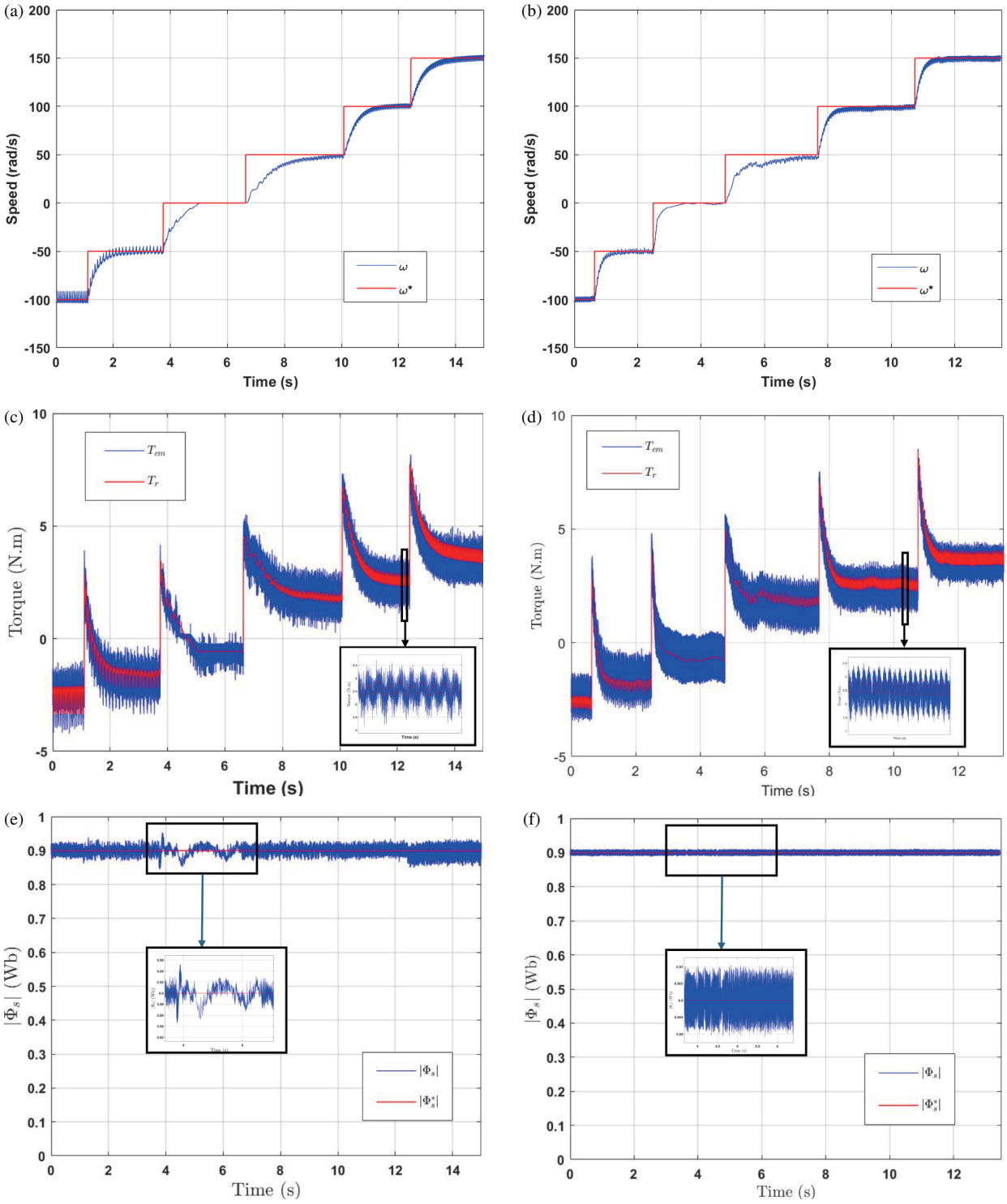

FIGURE 10. Speed, torque, and stator flux amplitude response during speed changes under constant load. (a) Speed and its reference (DTC-SVM). (b) Speed and its reference (FCS-MPC). (c) Torque and its reference (DTC-SVM). (d) Torque and its reference (FCS-MPC).(e) Stator flux amplitude and its reference (DTC-SVM). (f) Stator flux amplitude and its reference (FCS-MPC).

ics can be more easily filtered. In contrast, FCS-MPC control exhibits fewer significant harmonics, with most falling among the low-frequency harmonics, which are more challenging to filter. Therefore, while FCS-MPC appears to have a lower THD for the output voltage, the presence of low-frequency harmonics indicates that the DTC-SVM still offer advantages in terms of easier harmonic filtration, contributing to the lower current THD observed in DTC-SVM compared to FCS-MPC.

Figure 14 and 15 illustrate the results of two tests where the load charge changes rapidly first from no load to full load in Figure 14 and then from full load to no load in Figure 15 for both DTC-SVM and FCS-MPC, with the speed reference set

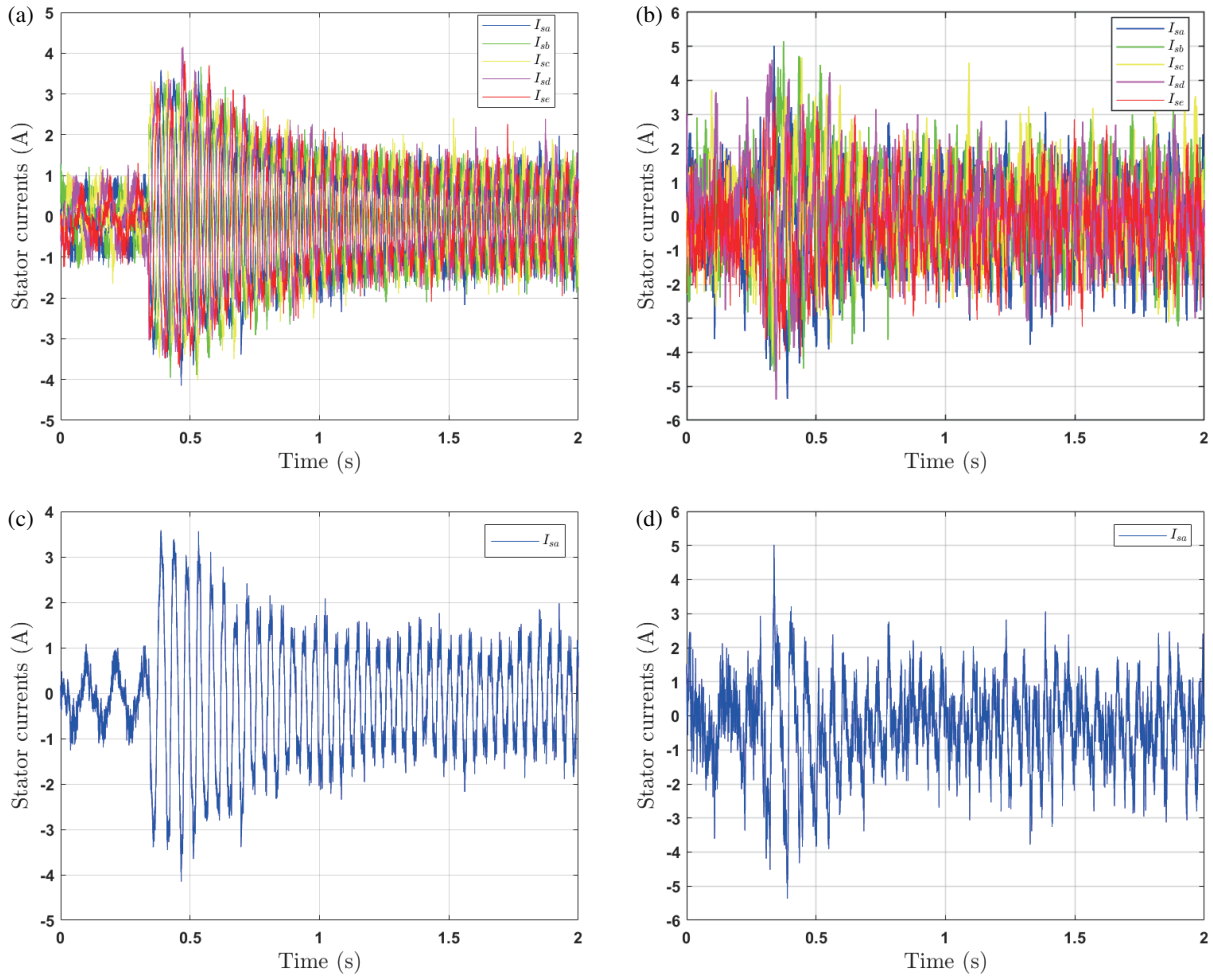

FIGURE 11. Stator currents. (a) Five-phase stator currents (DTC-SVM). (b) Five-phase stator currents (FCS-MPC). (c) Phase A stator currents (DTC-SVM). (d) Phase A stator currents (FCS-MPC).

TABLE 1. Comparative results between DTC-SVM and FCS-MPC for five-phase induction motors.

Parameter	DTC-SVM	FCS-MPC
Response Time (speed change)	Slower	Faster
Torque Ripple	Lower	Higher
Stator Flux Ripple	Higher	Lower
Stator Current Shape	Closer to sinusoidal	More variable
Peak Stator Current (transient)	3.3 A	5 A
Load Change Response (No Load to Full Load)	Higher drop in speed with longer recovery time	Smaller drop in speed with shorter recovery time
Load Change Response (Full Load to No Load)	Higher speed overshoot with longer recovery time	Smaller speed overshoot with shorter recovery time
THD of Stator Current	15.30%	22.85%
THD of Output Voltage	133.49% (most significant harmonics at medium and high frequencies)	94.33% (most significant harmonics at low frequency)

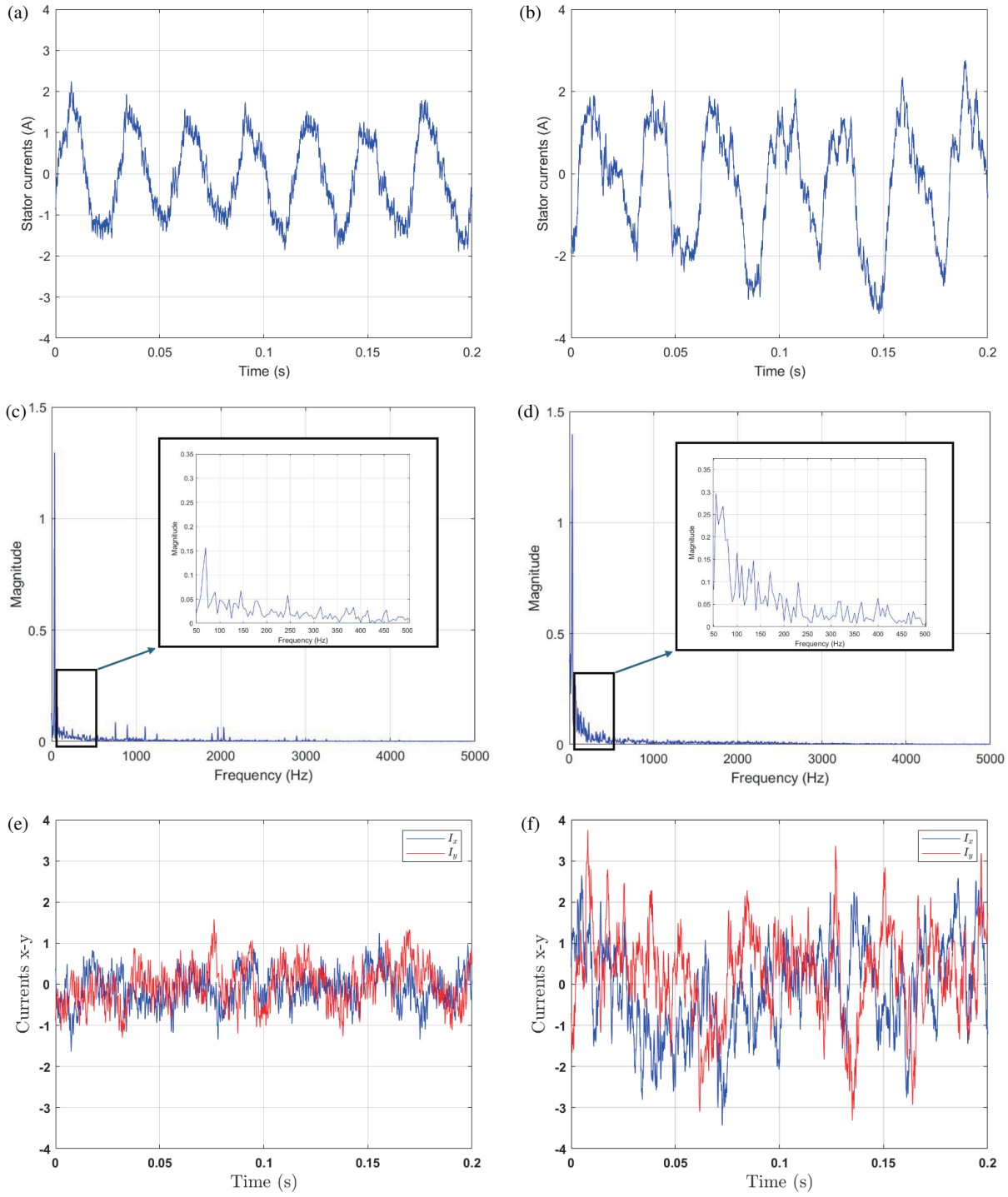

FIGURE 12. Harmonic analysis of the stator currents. (a) Phase A stator currents (DTC-SVM). (b) Phase A stator currents (FCS-MPC). (c) FFT of the stator currents (DTC-SVM). (d) FFT of the stator currents (FCS-MPC). (e) x-y current components (DTC-SVM). (f) x-y current components (FCS-MPC).

at 150 rad/s. In the first test, the torque responses shown in Figure 14(a) and Figure 14(b) indicate that both control strategies effectively handle the sudden load increase, with the actual torque T_{em} closely following the reference T_r. Correspondingly, the speed responses depicted in Figure 14(c) and Figure 14(d) reveal that DTC-SVM experiences a speed drop to 126 rad/s with a settling time of 4.8 seconds, whereas FCS-MPC shows a smaller speed drop to 132 rad/s with a faster recovery time of 4 seconds.

In the second test, where the load changes from full load to no load, the torque responses shown in Figure 15(a) and Figure 15(b) again demonstrate effective handling by both control strategies, with the actual torque T_{em} closely tracking the reference T_r. The speed responses depicted in Figure 15(c) and

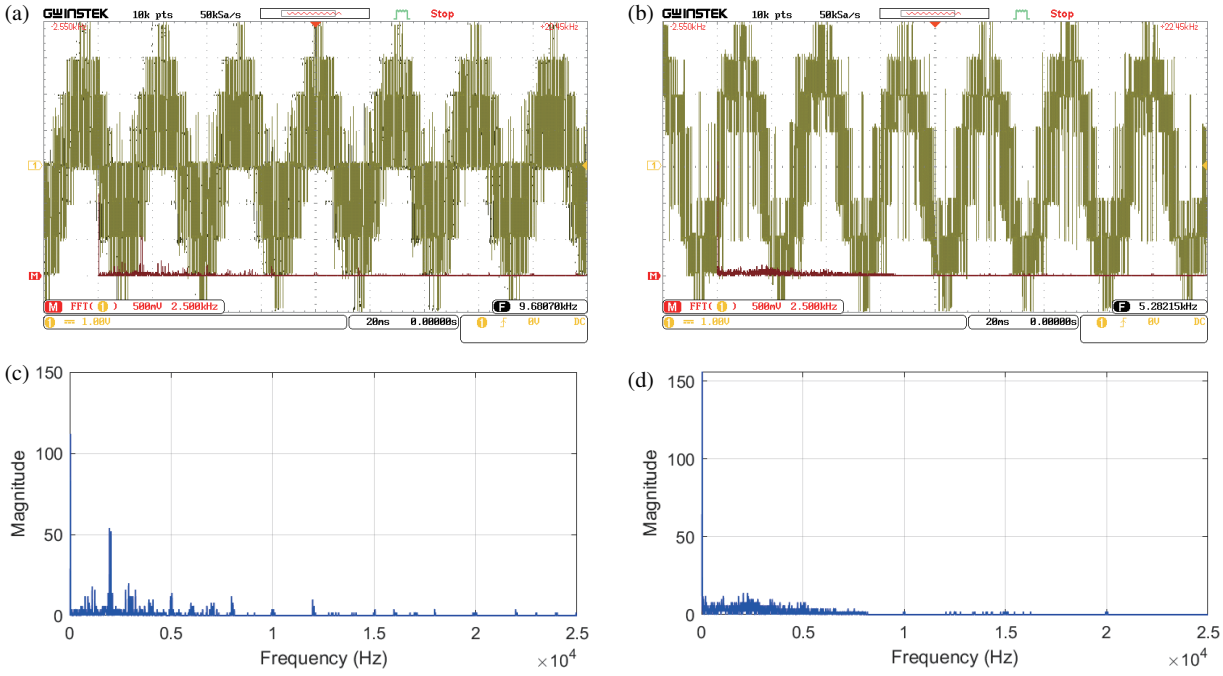

FIGURE 13. Harmonic analysis of the output voltage. (a) Output voltage (DTC-SVM). (b) Output voltage (FCS-MPC). (c) FFT of the output voltage (DTC-SVM). (d) FFT of the output voltage (FCS-MPC).

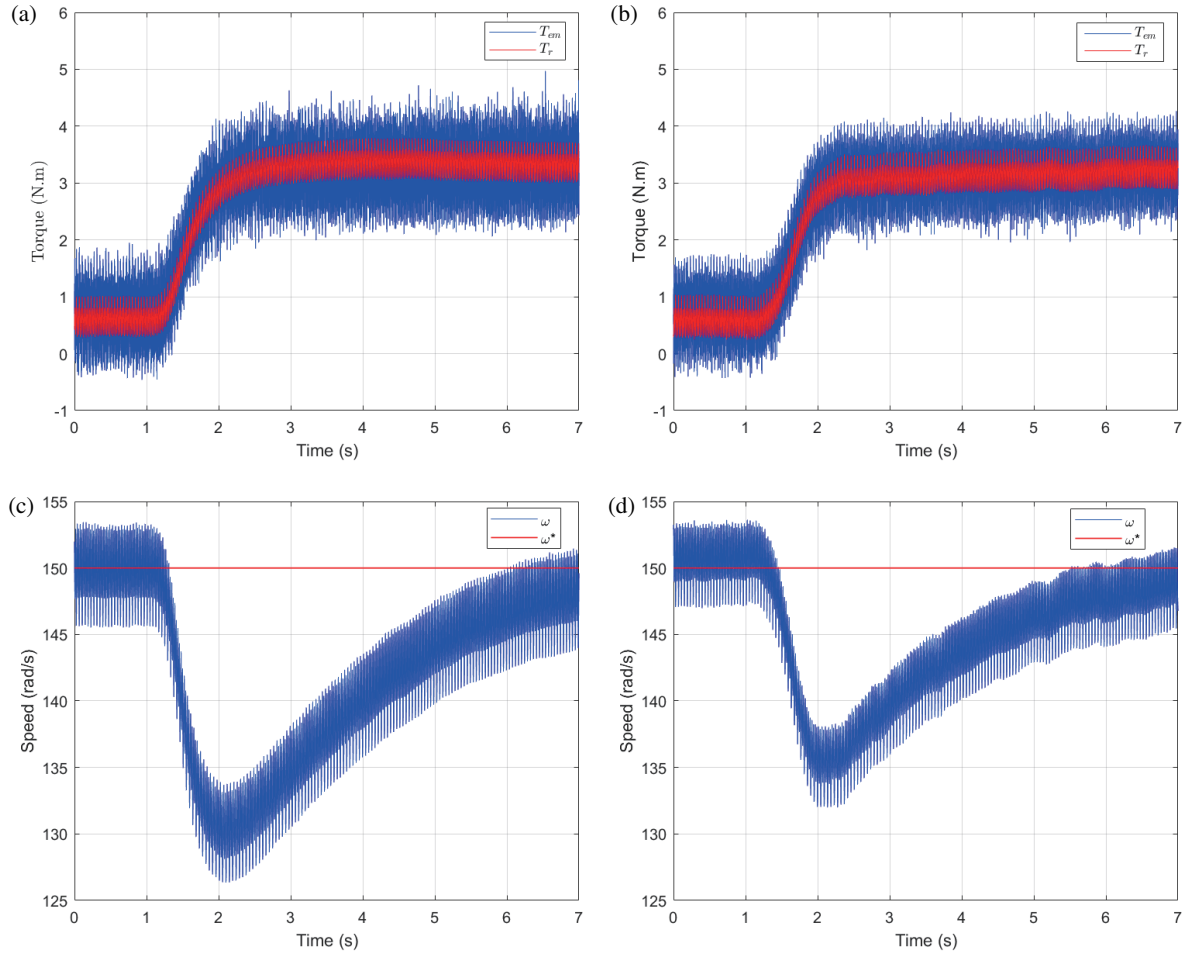

FIGURE 14. Torque and speed response during change from no load to full load. (a) Torque and its reference (DTC-SVM). (b) Torque and its reference (FCS-MPC). (c) Speed and its reference (DTC-SVM). (d) Speed and its reference (FCS-MPC).

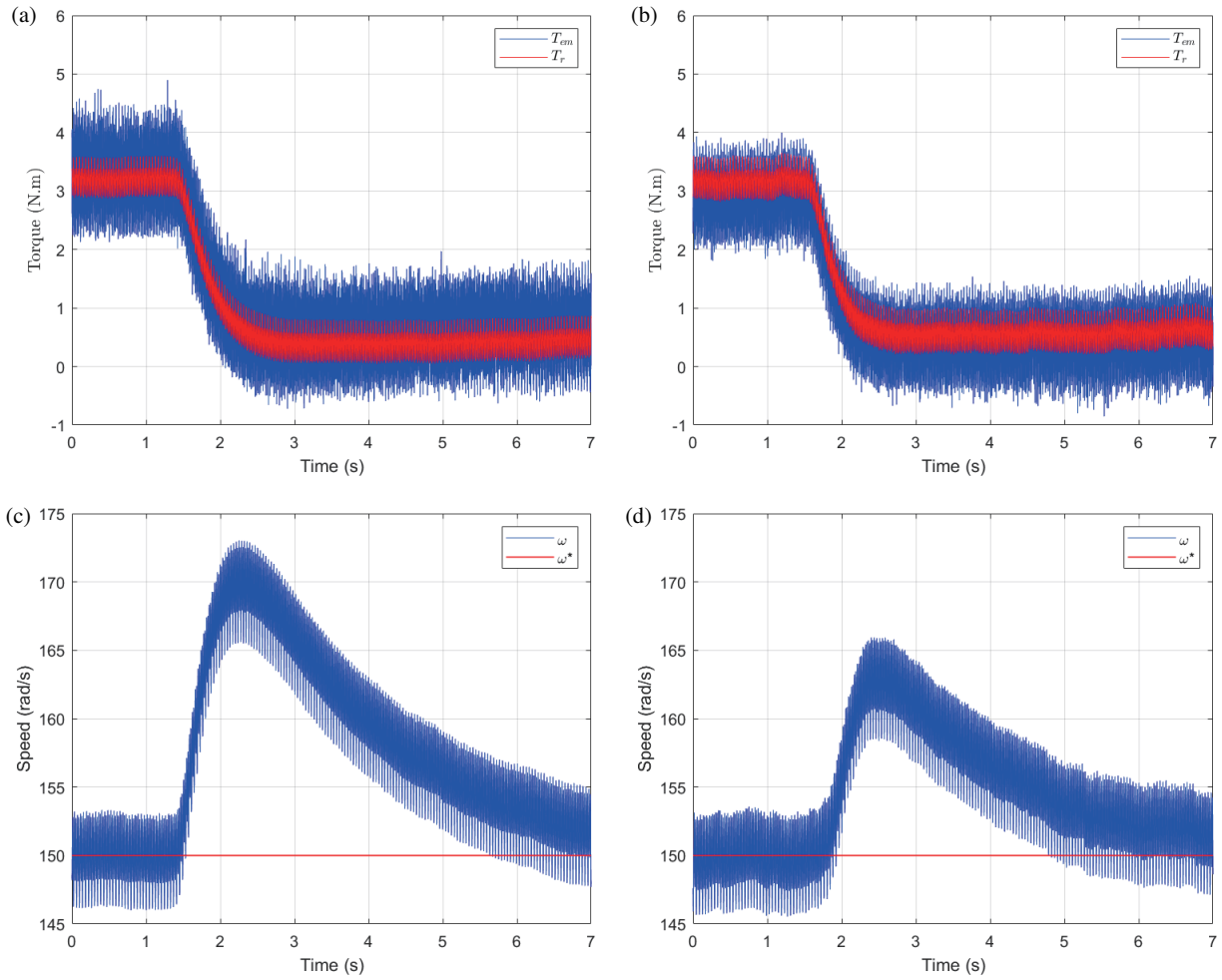

FIGURE 15. Torque and speed response during change from full load to no load. (a) Torque and its reference (DTC-SVM). (b) Torque and its reference (FCS-MPC). (c) Speed and its reference (DTC-SVM). (d) Speed and its reference (FCS-MPC).

Figure 15(d) indicate that DTC-SVM experiences a speed spike up to 173 rad/s with a recovery time of 4.2 seconds, while FCS-MPC shows a smaller spike to 166 rad/s and a quicker recovery time of 3 seconds.

Overall, these results highlight that while both DTC-SVM and FCS-MPC effectively manage sudden load changes, FCS-MPC consistently demonstrates superior performance with smaller speed fluctuations and faster recovery times in both load increase and decrease scenarios.

Table 1 summarizes the experimental findings comparing the performance of DTC-SVM and FCS-MPC control strategies for five-phase induction motors.

7. CONCLUSION

This comparative study between DTC-SVM and FCS-MPC for five-phase induction motors has yielded several key insights into the performance, efficiency, and control accuracy of these two advanced control strategies:

- **Dynamic Response**: FCS-MPC demonstrated a faster response time during changes in speed reference, along with smaller speed fluctuations and quicker recovery times during load variations, than DTC-SVM. This highlights the superior dynamic performance and robustness of FCS-MPC under transient conditions.
- **Torque Control**: Both DTC-SVM and FCS-MPC were effective in tracking the reference torque. However, DTC-SVM exhibited lower torque ripple, resulting in a smoother and more stable torque response. This indicates that DTC-SVM provides better torque control accuracy, especially during steady-state operations.
- **Stator Flux Control**: FCS-MPC showed superior control accuracy and stability in maintaining the desired stator flux magnitude, with minimal deviations even during speed variations.
- **Load Handling**: Both control strategies effectively managed sudden load changes, but FCS-MPC consistently showed smaller speed fluctuations and faster recovery times during both load increase and decrease scenarios. This indicates a higher level of robustness and efficiency in dealing with rapid load variations.

- **Harmonic Content**: The analysis of harmonic content shows that for the output voltage, DTC-SVM exhibits a higher THD with significant harmonics in the medium and high frequency ranges. In contrast, FCS-MPC shows a lower THD, but its harmonics are mainly in the low frequency range, primarily due to the variable switching frequency. While FCS-MPC appears to have a lower THD for the output voltage, the presence of low-frequency harmonics suggests that DTC-SVM offers advantages in easier harmonic filtration, contributing to its lower current THD compared to FCS-MPC.

In summary, while both DTC-SVM and FCS-MPC have their respective strengths, FCS-MPC demonstrates superior dynamic response, stator flux stability, and load handling capabilities. However, FCS-MPC's variable switching frequency leads to higher low-frequency harmonic content in the output voltage, which can be challenging to filter. On the other hand, DTC-SVM excels in torque control, offering lower torque ripple, and its fixed switching frequency results in smaller low-frequency harmonic content in the output voltage, effectively minimizing stator current harmonics. The choice between these strategies should consider specific application requirements, balancing the need for dynamic performance, torque stability, harmonic content, and load handling. This study not only offers valuable insights for optimizing the control of five-phase induction motors but also opens avenues for further research into optimizing these control methods or developing hybrid approaches that leverage the strengths of both to enhance the performance and efficiency of five-phase induction motor in various industrial applications.

APPENDIX A.

TABLE A1. Parameters for the five-phase induction motor and control settings used in experimental tests.

Parameter	Value	Parameter	Value
Pole pair number	1	P_{nom} [KW]	3.5
T_{nom} [N.m.]	12.7	R_s [Ω]	9.5
L_s [H]	1.389	L_m [H]	1.323
R_r [Ω]	7.3	L_r [H]	1.331
V_{dc} [V]	450	Switching period T_s [s]	0.001
PI Speed Controller P_{speed}	0.1	PI Speed Controller I_{speed}	0.05
PI Torque Controller P_{torque}	120	PI Torque Controller I_{torque}	50
PI Flux Controller P_{flux}	1000	PI Flux Controller I_{flux}	80

REFERENCES

[1] Kulandaivel, G., E. Sundaram, M. Gunasekaran, and S. Chenniappan, "Five-phase induction motor drive — A comprehensive review," *Frontiers in Energy Research*, Vol. 11, 1178169, 2023.

[2] Xu, H., H. A. Toliyat, and L. J. Petersen, "Five-phase induction motor drives with DSP-based control system," *IEEE Transactions on Power Electronics*, Vol. 17, No. 4, 524–533, 2002.

[3] Duran, M. J., F. Salas, and M. R. Arahal, "Bifurcation analysis of five-phase induction motor drives with third harmonic injection," *IEEE Transactions on Industrial Electronics*, Vol. 55, No. 5, 2006–2014, 2008.

[4] Kellner, J., S. Kaščák, and Z. Ferková, "Investigation of the properties of a five-phase induction motor in the introduction of new fault-tolerant control," *Applied Sciences*, Vol. 12, No. 4, 2249, 2022.

[5] Xu, H., J. Zhao, L. Yang, H. Chen, X. Luo, and S. Zhang, "Research on open circuit fault modeling and fault tolerant control strategy of five-phase induction motor," *Processes*, Vol. 10, No. 9, 1891, 2022.

[6] Mossa, M. A. and H. Echeikh, "A novel fault tolerant control approach based on backstepping controller for a five phase induction motor drive: Experimental investigation," *ISA Transactions*, Vol. 112, 373–385, 2021.

[7] Levi, E., "Multiphase electric machines for variable-speed applications," *IEEE Transactions on Industrial Electronics*, Vol. 55, No. 5, 1893–1909, 2008.

[8] Iffouzar, K., B. Amrouche, T. O. Cherif, M.-F. Benkhoris, D. Aouzellag, and K. Ghedamsi, "Improved direct field oriented control of multiphase induction motor used in hybrid electric vehicle application," *International Journal of Hydrogen Energy*, Vol. 42, No. 30, 19 296–19 308, 2017.

[9] Duran, M. J. and F. Barrero, "Recent advances in the design, modeling, and control of multiphase machines — Part II," *IEEE Transactions on Industrial Electronics*, Vol. 63, No. 1, 459–468, 2016.

[10] Gaikwad, S. A. and S. M. Shinde, "Review on five-phase induction motor fed by five-phase voltage source inverter with different conduction mode," in *2020 International Conference on Industry 4.0 Technology (I4Tech)*, 199–202, Pune, India, 2020.

[11] Lu, S. and K. Corzine, "Direct torque control of five-phase induction motor using space vector modulation with harmonics elimination and optimal switching sequence," in *Twenty-First Annual IEEE Applied Power Electronics Conference and Exposition, 2006. APEC '06.*, 7, Dallas, TX, USA, Mar. 2006.

[12] Khaldi, B. S., A. Kouzou, M. O. Mahmoudi, and D. Boukhetala, "DTC-SVM sensorless control of five-phase induction motor based on two different rotor speed estimation approaches," *Nonlinear Dynamics and Systems Theory*, Vol. 21, No. 3, 262–279, 2021.

[13] Khaldi, B. S., H. Abu-Rub, A. Iqbal, R. Kennel, M. O. Mahmoudi, and D. Boukhetala, "Comparison study between a simple sensorless method and adaptive observer for DTC-SVM five-phase induction motor drive," in *2012 IEEE International Conference on Industrial Technology*, 743–748, Athens, Greece, 2012.

[14] Listwan, J. and K. Pieńkowski, "DTC-ST and DTC-SVM control of five-phase induction motor with MRAS^{CC} estimator," *Przegląd Elektrotechniczny*, Vol. 92, No. 11, 252–256, 2016.

[15] Barik, S. K. and K. K. Jaladi, "Five-phase induction motor DTC-SVM scheme with PI controller and ANN controller," *Procedia Technology*, Vol. 25, 816–823, 2016.

[16] Benyoussef, E. and S. Barkat, "DTC-SVM of sensorless five-phase induction machine using extended Kalman filter," *International Journal of Circuits, Systems and Signal Processing*, Vol. 17, 143–152, 2023.

[17] Lim, C. S., E. Levi, M. Jones, N. A. Rahim, and W. P. Hew, "Experimental evaluation of model predictive current control of a five-phase induction motor using all switching states," in *2012 15th International Power Electronics and Motion Control Conference (EPE/PEMC)*, LS1c–4, Novi Sad, Serbia, Sep. 2012.

[18] Lim, C. S., E. Levi, M. Jones, N. A. Rahim, and W. P. Hew, "FCS-MPC-based current control of a five-phase induction motor and its comparison with PI-PWM control," *IEEE Transactions on Industrial Electronics*, Vol. 61, No. 1, 149–163, 2014.

[19] Guzman, H., M. J. Duran, F. Barrero, B. Bogado, and S. Toral, "Speed control of five-phase induction motors with integrated open-phase fault operation using model-based predictive current control techniques," *IEEE Transactions on Industrial Electronics*, Vol. 61, No. 9, 4474–4484, 2014.

[20] Martín, C., M. R. Arahal, F. Barrero, and M. J. Durán, "Five-phase induction motor rotor current observer for finite control set model predictive control of stator current," *IEEE Transactions on Industrial Electronics*, Vol. 63, No. 7, 4527–4538, 2016.

[21] Guzman, H., A. Iqbal, and F. Barrero, "Reduction of common-mode voltage using a simplified FSC-MPC for a five-phase induction motor drive," *The Journal of Engineering*, Vol. 2019, No. 17, 3772–3777, 2019.

[22] Levi, E., R. Bojoi, F. Profumo, H. A. Toliyat, and S. Williamson, "Multiphase induction motor drives — A technology status review," *IET Electric Power Applications*, Vol. 1, No. 4, 489–516, 2007.

[23] Gaikwad, S. A. and S. M. Shinde, "Five-phase induction motor modeling and its analysis using matlab/simulink," in *Smart Technologies for Energy, Environment and Sustainable Development*, Vol. 1, 645–654, 2022.

[24] Iqbal, A., S. M. Ahmed, M. A. Khan, M. R. Khan, and H. Abu-Rub, "Modeling, simulation and implementation of a five-phase induction motor drive system," in *2010 Joint International Conference on Power Electronics, Drives and Energy Systems & 2010 Power India*, 1–6, New Delhi, India, 2010.

[25] Aher, K. S. and A. G. Thosar, "Modeling and simulation of five-phase induction motor using MATLAB/Simulink," *International Journal of Engineering Research and Applications*, Vol. 6, No. 5, 1–8, 2016.

[26] Lai, Y.-S. and J.-H. Chen, "A new approach to direct torque control of induction motor drives for constant inverter switching frequency and torque ripple reduction," *IEEE Transactions on Energy Conversion*, Vol. 16, No. 3, 220–227, 2001.

[27] Sabri, S., A. Benachour, H. E. Guessar, M. L. Badaoui, E. M. Berkouk, M. O. Mahmoudi, M. Kermadi, and S. Mekhilef, "Analysis and assessment of electrical and thermal performance of five-phase voltage source inverter under different modulation strategies: Comparative study under balanced and unbalanced load," *International Journal of Circuit Theory and Applications*, Vol. 52, No. 9, 4254–4281, 2024.

[28] Iqbal, A. and M. A. Khan, "A simple approach to space vector PWM signal generation for a five-phase voltage source inverter," in *2008 Annual IEEE India Conference*, Vol. 2, 418–424, Kanpur, India, 2008.

[29] Mekhilef, A. A., A. Benachour, E. M. Berkouk, and A. Dali, "FCS-MPC of a DMC-fed induction machine with unity input power factor using rotating vectors," in *2021 21st International Symposium on Power Electronics (Ee)*, 1–6, Novi Sad, Serbia, 2021.